Arecibo observations of ionospheric perturbations associated with the passage of Tropical Storm Odette

R. L. Bishop,[1,2] N. Aponte,[3] G. D. Earle,[4] M. Sulzer,[3] M. F. Larsen,[1] and G. S. Peng[5]

[1]   A suite of instruments including incoherent scatter radar, ionosonde, and a satellite-bourne GPS receiver observed the ionosphere immediately following the passage of a tropical storm. Tropical Storm Odette formed on 4 December 2003 and proceeded northeasterly over the next 4 days, passing within 600 km of the Arecibo Observatory (AO). On the night of 7−8 December AO measured F region plasma densities and velocities nearly coincident with the storm. Large velocity variations, 10−80 m/s, are evident in the plasma drift components. The variations appear wave-like with an average period of 90 min at 367 km. Zonal drifts were observed with magnitudes significantly greater than commonly observed for similar geomagnetic conditions. The Ramey ionosonde observed intense midlatitude spread F on the night following the closest passage of the storm. GPS occultations within the storm path showed an increase in gravity wave activity and F region scintillation. Combining the local increase in gravity wave activity with the large drift variations and dominant meridional electric field observed immediately following the storm's traversal of the flux tube coincident with the AO observing volume provide insight into coupling between mesoscale weather systems and the ionosphere.

1.   Introduction

[2]   Gravity waves generated at lower altitudes are commonly cited as the cause of disturbances observed in the airglow layer, ionospheric plasma, and neutral wind field in the upper atmosphere and thermosphere [e.g., *Goodwin*, 1980; *Kazimirovsky et al.*, 2003; *Lastovicka*, 2006]. Studies of tropospheric thunderstorms have shown gravity wave generation and propagation into the stratosphere and thermosphere [e.g., *Röttger*, 1977; *Larsen et al.*, 1982; *Boeck et al.*, 1995; *Vadas and Fritts*, 2004, 2006]. Other studies have indicated that wave generation from weather systems moving over the Andes mountain range may perturb the local ionosphere [*Mazano et al.*, 1998]. Observational evidence of thunderstorm-produced ionospheric effects has also been documented by sounding rocket measurements [*Kelley et al.*, 1985; *Kelley*, 1997].

[3]   Since hurricanes and tropical storms create numerous thunderstorms and intense convection regions over an extended horizontal area, significant gravity wave generation above such storms is expected. If notable coupling between the troposphere and ionosphere exists, these large storms should provide an ideal source for ionospheric perturbations. Approximately eight hurricanes or tropical storms form in the Atlantic region and approach the U.S. coast each year. Of these, 2−3 typically pass within 500 km of the Arecibo Observatory.

[4]   *Bauer* [1958] was the first to observe a possible ionospheric response following the nearby passage of a hurricane. Utilizing ionosonde data during the passage of four hurricanes, Bauer showed an increase in $f_{o}F_{2}$ with the approach of the storms. *Hung and Kuo* [1978] presented HF radar data of tropospheric gravity waves and ionospheric motions associated with Hurricane Eloise. Their study observed wave-like fluctuations at F region altitudes with horizontal wavelengths on the order of 100 km. Using group ray tracing, they showed that the source of gravity waves propagating to the ionosphere was located along the storm track.

[5]   Tropical Storm (TS) Odette formed in the western Caribbean on 4 December 2003. Formation of tropical storms in the western Caribbean late in the season is extremely rare. Only eight tropical storms/hurricanes have formed in the month of December since records began in 1871. Of these, only a tropical storm in 1887 and the 2003 storms Odette and Peter initially formed in the Caribbean. Over the 4 days following its formation, the storm track of Odette was directed northeast, and the storm passed within 600 km of Puerto Rico. On 7 December the night immediately following Odette's closest approach to the island, the

[1]Department of Physics, Clemson University, Clemson, South Carolina, USA.

[2]Currently at The Aerospace Corporation, El Segundo, California, USA.

[3]NAIC, Arecibo, Puerto Rico, USA.

[4]William B. Hanson Center for Space Sciences, University of Texas at Dallas, Richardson, Texas, USA.

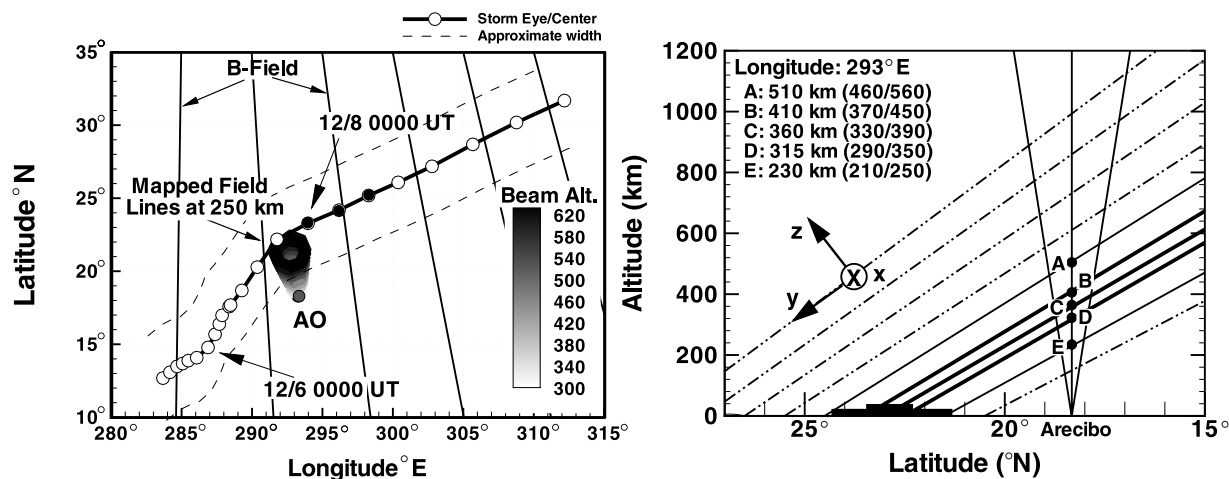[5]The Aerospace Corporation, El Segundo, California, USA.

Figure 1. The left panel shows the path of Tropical Storm Odette from 5 to 9 December 2003 along with the location of the Arecibo Observatory (AO). The circles depict observations of the storm position made approximately every 5–6 hours; the solid circles indicate the position of the storm during the radar observation period. The shaded cone represents the footprint of the observed B-field lines mapped to 250 km. The right panel depicts the storm orientation to the B-field lines at 293°E longitude. The filled rectangles represent the storm eye and approximate overall horizontal extent of the storm. The solid B-field lines represent the lines crossed by the storm eye. The vertical AO line-of-sight is shown with the geomagnetic field intersections labeled A–E and the values listed. The 15° AO lines of sights are also shown with the left and right intersection altitudes listed in parenthesis, respectively. The arrows near 300 km in the right panel shows the geomagnetic coordinate system used throughout the paper.

Arecibo Observatory (AO) made ionospheric observations for over six hours. This paper presents AO observations showing significant variations in all three plasma drift components as a function of both time and altitude during this period.

2. Experiment Description and Observations

[6] The left panel of Figure 1 illustrates the storm track of Tropical Storm Odette over an approximately 4-day period. The dots along the track signify the actual position in UT as measured every 6 hours by the National Weather Service and NOAA. To convert from UT to AST, subtract 4 hours. The Arecibo Observatory is denoted as a single black dot. The filled circles along the storm path indicate Odette's position during the AO observation period on 7–8 December. The right panel of Figure 1 displays the approximate B-field lines at 293°E longitude, the location and diameter of Odette and the storm's eye (filled rectangles), and the intersect altitude of the vertical and ±15° AO beam.

[7] During the observing period on 7–8 December, the eye of Tropical Storm Odette was located 530–675 km from AO. The Arecibo radar observed ionospheric plasma density and drift velocities for approximately 6 hours on the night of 7–8 December 2003. The AO beam was directed 15° off vertical and swept 360° in azimuth. This mode provided measurements of the plasma Doppler drifts in all three-dimensions [Hagfors and Behnke, 1974; Sulzer et al., 2005]. The data are averaged over 60 s intervals and broken into 5° azimuth bins. The local electric field is calculated using $\vec{E} + (\vec{v} \times \vec{B}) = 0$. In the F region, where plasma collisions are infrequent, any observed plasma motion perpendicular to the magnetic field in the region may be interpreted as resulting from the presence of a perpendicular electric field. In the left panel of Figure 1, the shaded cone represents the magnetic field lines that are intersected by the radar beam as mapped to 250 km. The x-, y-, z-coordinate system shown in the right panel of Figure 1 shows the geomagnetic coordinate system used throughout the paper. The x, y, z directions correspond to the geomagnetic zonal, meridional, and antiparallel with respect to magnetic field lines directions, respectively.

[8] Geomagnetic activity was moderate during the observation period with a daily average Ap of 14 and 35 for 7 and 8 December, respectively. The 3-hour Kp values from 2100 7 December to 0900 8 December are moderate: 3+, 2+, 4+, and 4. Figure 2 shows the 3-hour Kp, daily averaged Ap, and hourly averaged Dst values for the first half of December 2003. First-look AE values from the Kyoto world data center shows little activity at the beginning of the observation window with values of less than 250 nT between 0 and 3.5 UT. Data from the ACE satellite showed the Bz component of the IMF field to be approximately 4 nT northward at the beginning of the period, steadily decreasing to approximately 4 nT southward by 0800 UT (*ACE Data Center*, http://www.srl.caltech.edu/ACE/ASC/). From 2100 to 0500 7–8 December, Dst steadily increased from −34 to −26 nT. The Dst value then decreased to −35 nT. The observation period occurred 72 hours after a Class 1 moderate storm and 5 hours after a weak storm, following the classification of *Yokoyama and Kamide* [1997]. Thus it can be concluded that prompt penetration electric field conditions were not present.
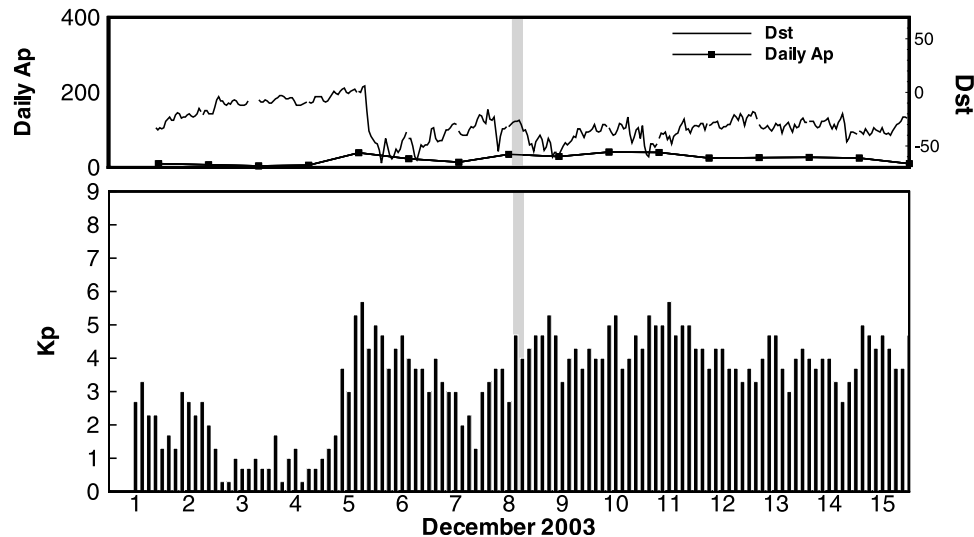
Figure 2. The top panel shows the Ap daily average values and the 1 hour average Dst values for the first half of December. The bottom panel displays the 3-hour Kp values. The gray shadings denote the approximate AO observation period. All times are in UT.

[9] Figure 3 shows the altitude and density at the F peak in the top and bottom panels, respectively. The F peak is above 400 km at the beginning of the observation period. It then descends nearly 200 km over the next 3 hours. From 0500 to 0700 UT the F peak exhibits a slightly downward motion but remains between 230 and 270 km. The bottom panel showing the peak density exhibits nearly the opposite behavior. From 0200 to 0430 UT the density steadily increases, reaching a maximum near 0445 UT. The density remains relatively steady until 0600 UT and then decreases. The 15 min variations clearly observed in the density data and somewhat visible in the altitude data are due to the azimuthal scans of the radar. At 0445 UT the

density variation implies that the F peak density varies by 2e5 cm^{-3} over 150 km horizontal distance.

[10] Figure 4 shows the range-time-intensity (RTI) plot for the 80–160 km altitude range. This region contains several sporadic-E (Es) layers and one intermediate layer [*Mathews*, 1998]. The 15 min variations are again due to the azimuthal radar scans. However, the clear altitude variations due to the scan imply that the intermediate and the Es layers are tilted with respect to the horizontal.

[11] Several interesting features are visible in both layer types. First, there is large scale altitude motion of the higher-altitude sporadic E layer. The Es layer reaches the lowest altitude near 0300 UT of 104 km. It then increases to
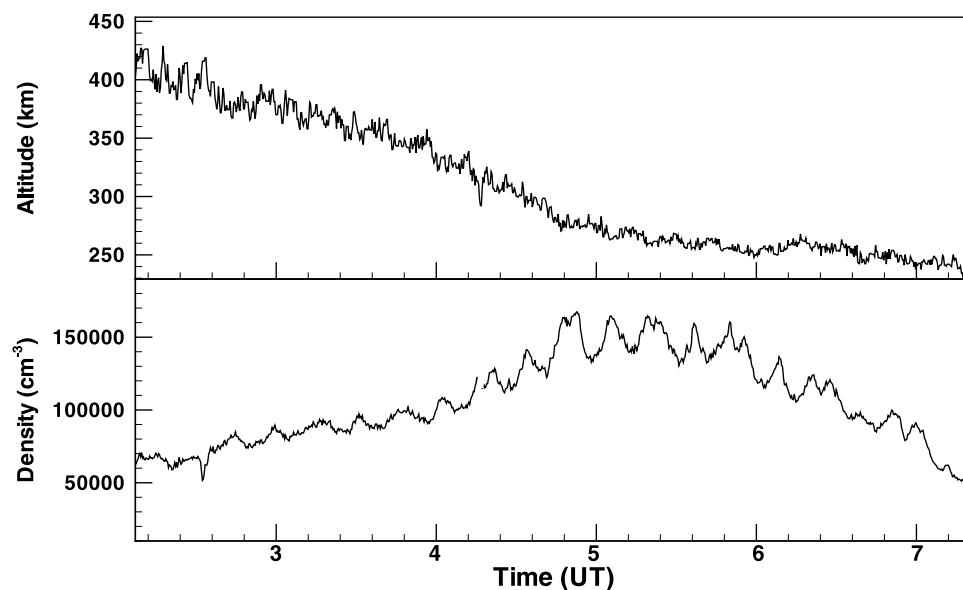

Figure 3. The top panel shows the altitude variation of the F-peak during the observation window. The bottom panel shows the variations in the F-peak density as a function of time. The 15-min wave-like variations are the result of the radar beam sweeps.
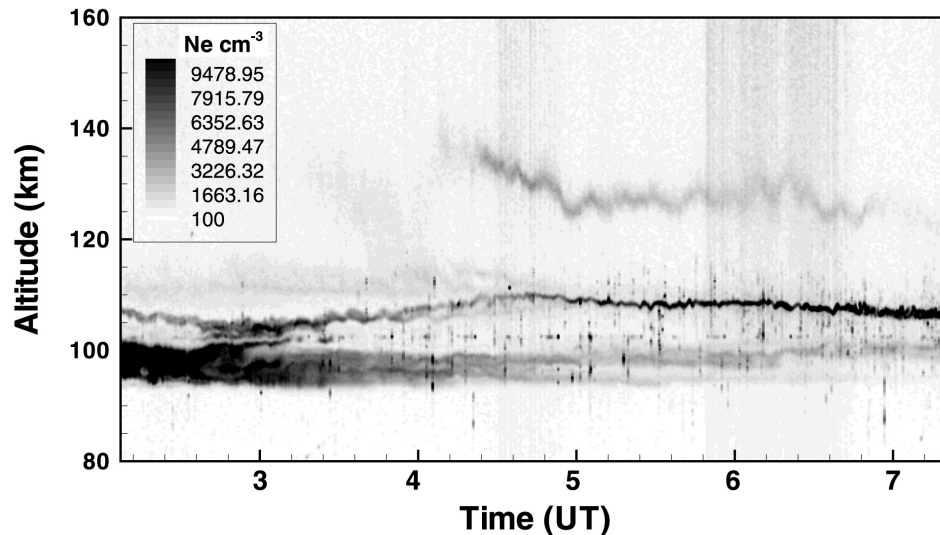
Figure 4. The plot shows a range-time-intensity (RTI) plot of the sporadic E and intermediate layers observed on 7–8 December 2003. The 15-min wave-like variations are the result of the radar beam-sweeps.

approximately 110 km at 0440 UT. For the last few hours the Es layer remains relatively steady in altitude. The Es layer near 100 km appears to be over 5 km thick prior to 0300 UT. After 0300 UT, the layer density decreases and the thick layer resembles two or more thin Es layers. The intermediate layer occurs coincident to the increase in F peak density as shown in the bottom panel of Figure 3. The motion of the layers is likely due to the passage of gravity waves and will be discussed in detail in the next section.

[12] Figure 5a shows the plasma drifts observed by AO at 367 km over the entire evening. Positive values in Figure 5a represent zonal (magnetic east), meridional (magnetic north), and antiparallel direction. Large fluctuations are observed in all three components with the drift component along B consistently parallel or downward. Figure 5b shows the observed meridional drifts. Also shown in Figure 5 are the average drifts near December solstice for high (dashed) and low (dash-dot-dot) solar activity as adapted from *Fejer* [1993]. The meridional drift is initially southward and then switches to northward near local midnight. This overall behavior is similar to that displayed by the average drift. However, the observed meridional drift shows more variations over the 6-hour period. Additionally, during the first hour of observations the observed meridional drift has a magnitude more than three times greater than the averages shown. It should be noted that during the first 15 min the measurements have a larger standard deviation due to fewer data points in the beam-swinging experiment. Figure 5c shows the observed zonal drifts and the average drifts from *Fejer* [1993], similar to Figure 5b. The zonal drift reaches a maximum of 105 m/s eastward prior to local midnight and then completely changes direction in the next hour, remaining westward for the rest of night. The general trend is similar to the average drift profiles, but the observed profile reaches a maximum eastward drift more than four times the average. Two hours later, it reverses back to the west.

[13] Figure 6 shows the total horizontal electric field mapped to an altitude of 250 km as a function of geographic latitude and longitude. Each panel in Figure 6 shows the vector electric field for one complete azimuthal scan with the exception of the first panel which shows the initial partial scan. The colored arrows designate the altitude at which the radar beam observed the original plasma drift. The data has been limited to nine altitudes, between 293 and 590 km, where significant plasma density was present. The length and color of the arrows denote the magnitude and altitude of the E-field, respectively. The nine panels are separated by 8–9 min. In the bottom left corner of each panel the height of the F2 peak (hF2) and the distance between the observatory and storm eye (D_{A-O}) are listed.

[14] The calculated electric field directions vary in time and by altitude within a given panel. Beginning at 0207 LT, the flow direction varies with altitude with the lowest altitudes tending southward and the higher altitudes north-westward. In the first two panels, 0207–0223 UT, the vector directions appear somewhat divergent with the source somewhere east of 294°E longitude at an altitude near 479 km, and in the general direction of Odette. By 0232 UT, the electric field appears to be changing more smoothly over all altitudes. However, even during this scan there appears to be a divergent source centered at a higher altitude between 516 and 553 km. From 0335 to 0358 UT the direction of the E-field at 553 km appears anomalous. The direction is northeast while the electric fields at altitudes below 553 km are nearly north. At altitudes above 553 km, the field varies from northeast at 0335 UT to northwest at 0351 UT. In the last panel, the highest altitude, 590 km, exhibits a significantly different direction then observed in the other altitudes.

[15] The electric field magnitudes also vary in altitude and time. The electric field magnitude below the F peak within the first 45 min was 4–5 mV/m. At the F peak during the same period the electric field ranges between
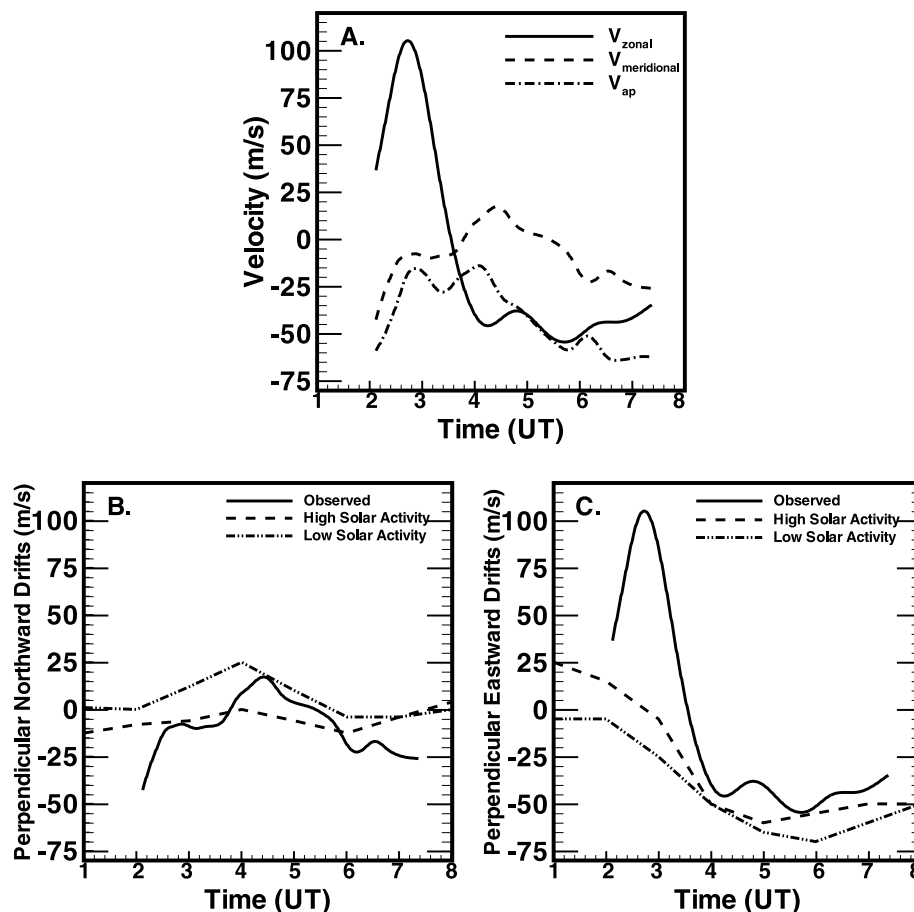
Figure 5. (a) The three components of the ion drift velocities as measured by AO. (b (c)) The observed meridional (zonal) drifts perpendicular to the geomagnetic field along with the average drifts for low and high solar activity adapted from *Fejer* [1993].

2 and 3 mV/m. As the evening progresses the electric field magnitude decreases at all altitudes, reaching a minimum near 0335 UT of less than 0.5 mV/m. In the last two panels the electric field begins to increase in strength with similar magnitudes 1–1.5 mV/m at all altitudes.

[16] In addition to radar data, limited GPS radio occultation (GPSRO) data are available. Table 1 lists characteristics of occultations obtained by the CHAMP satellite near the storm. The CHAMP satellite launched in 2000 into a circular orbit at 454 km. The onboard GPS receiver observes approximately 500 occultations a day. A more complete description of the mission, GPS instrument, and data can be found in the work of *Wickert et al.* [2001]. Figure 7 shows an example of an atypical tropospheric profile (solid line) observed within the path of the storm. The dashed line in Figure 7 is the temperature profile obtained from MSIS for the same time and conditions. The two temperature profiles show very different tropopauses. The MSIS tropopause occurs near 16 km at a temperature of −60°C. The occultation temperature profile is unusual. First, the minimum temperature of the tropopause is −80°C near 18 km. This minimum temperature is not only much colder than the typical climatology for this time of year but exceeds the average minimum temperature found during the winter months [*Holton*, 1992]. Second, a "double" tropopause consistent with a tropopause fold

occurs near 15 km, indicative of dynamic coupling between the stratosphere and troposphere. Tropospheric folds have been observed associated with cyclones [*Uccellini et al.*, 1985]. They are strongly influenced by mesoscale vertical circulations, often forcing stratospheric air to lower altitudes. Thus the large tropopause fold shown in Figure 7 likely indicates either significant gravity waves or mesoscale dynamics leading to gravity wave generation. Some possible gravity wave oscillations are observed near 20 km, as shown in Figure 7. Longer wavelength gravity waves cannot be observed since the useable altitude range of the GPSRO extends only to 25 km at the lower altitudes.

3. Discussion

[17] The Arecibo measurements presented here reveal some unusual behavior in the F region plasma drifts. As mentioned previously, Figure 5 shows large zonal drifts with significant variations. For 2 + < Kp < 4, the average perpendicular zonal nighttime drifts above Arecibo tend to be westward with magnitudes less than about 50 m/s [*Ganguly et al.*, 1987]. The observed zonal drifts at 367 km shown in Figure 5a is eastward for almost 90 min with a maximum magnitude velocity twice that of the average. On average, the zonal drift at AO normally does not exceed 80 m/s even during intense geomagnetic
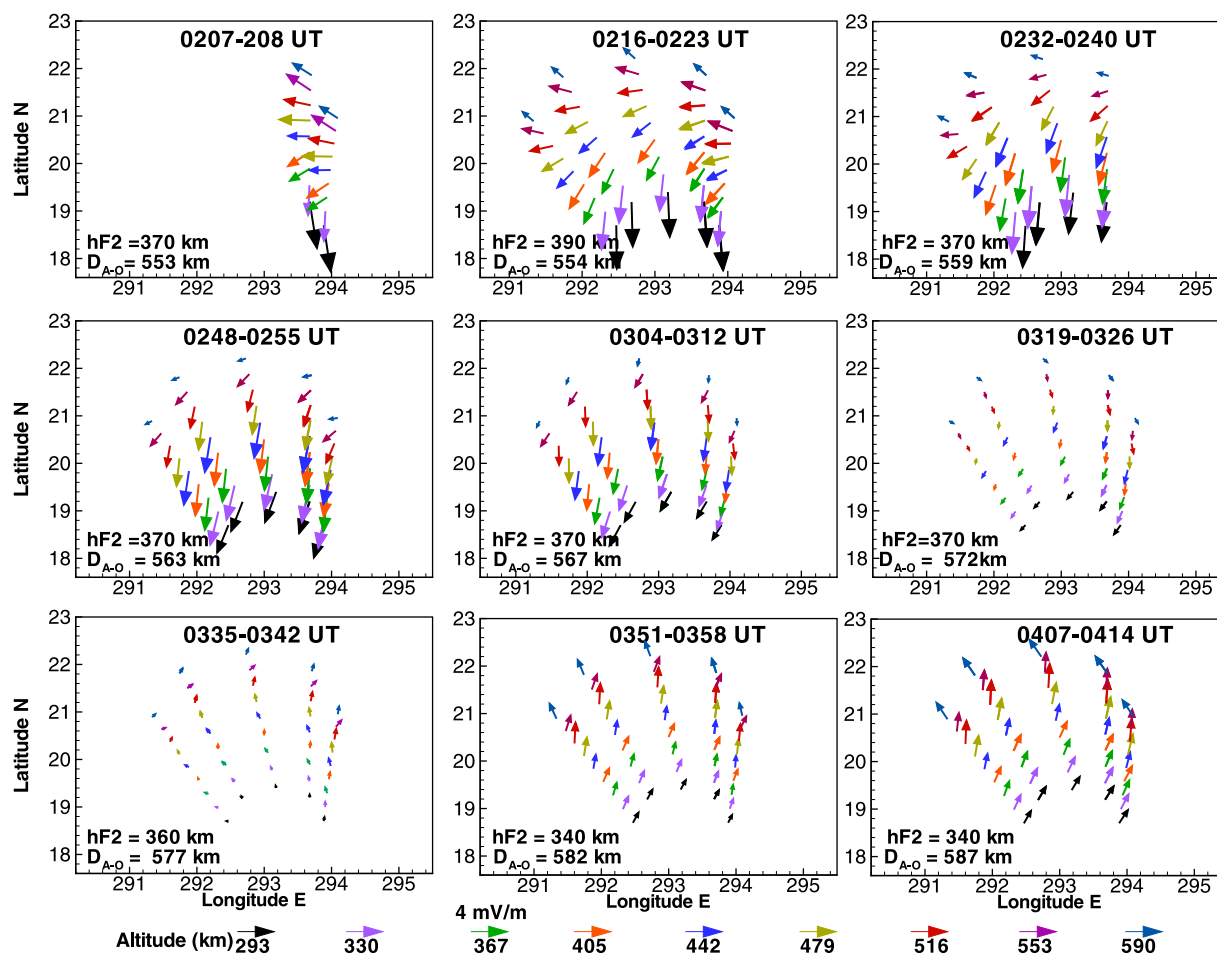
Figure 6. The total horizontal electric fields mapped to 250 km are shown as a function of latitude and longitude. D_{A-O} is the distance between the storm eye and the Arecibo Observatory. Each color represents a different altitude along the radar beam path and the length of the arrows indicates the relative strength of the field.

conditions [*Fejer and Emmert*, 2003; *Pi et al.*, 2000]. After 0300 LT the zonal drift is more typical with westward flow and a magnitude between 35 and 50 m/s. The average perpendicular meridional drifts for the same Kp interval tend to be southward premidnight and northward postmidnight with magnitudes less than 10 m/s [*Ganguly et al.*, 1987]. It should be noted that the average zonal flow at high solar activity is eastward until 0300 LT (as shown in Figure 5c), but the maximum velocity is nearly four times less than that observed during the same time period. The observed zonal drift is in the same direction and has magnitudes similar to the average drift

values. Although it might be possible for intense geomagnetic activity to cause the observed large drifts, the subsequent temporal variations observed in all three-drift components cannot be explained by geomagnetic conditions. During the first hour when the large zonal and meridional drifts are observed, the Es layer in Figure 4 showed a large-scale altitude variation. The simultaneous motion of the *F* region and Es layers further demonstrates coupling between the various altitude regions.

[18] At night over Arecibo, the quiet time electric fields are expected to be predominantly in the zonal direction [*Fejer*, 1993]. Figure 6 shows that a southward meridional

Table 1. Characteristics of Troposphere/Stratosphere and Ionospheric CHAMP GPS Occultation Profiles Near Tropical Storm Odette[a]

Date	Time, UT	PRN	Latitude, °N	Longitude, °E	Approx. Distance to Storm, km	Double Tropopause?, Depth °C	Stratosphere G.W. Ave. λ, km	*F* Region Scintillation
12/6/03	0127	26	16.7	295.3	700	Y (1.78)	1.8	Y
12/8/03	0108	26	12.6	296.3	1200	N	2.0	Y
12/8/03	0245	7	34.7	296.3	1000	Y (1.66)	2.3	Y
12/8/03	1400	30	29.0	305.4	150	Y (9.52)	1.7	Y

[a]Tropospheric data obtained at the CHAMP data center http://isdc.gfz-potsdam.de/champ/). Ionospheric data processed at The Aerospace Corporation.
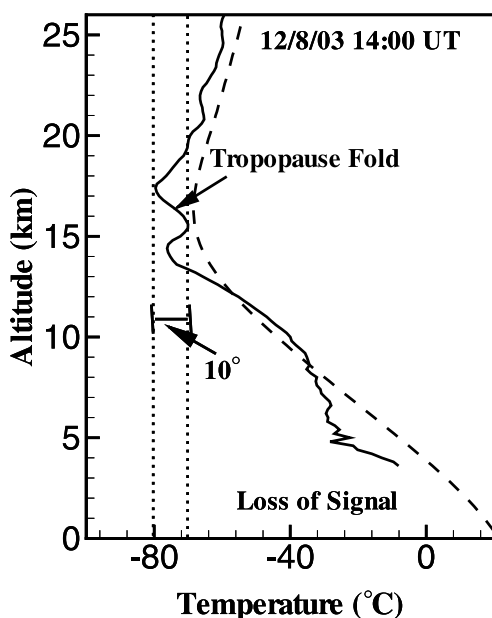
Figure 7. The plot shows a temperature profile from a CHAMP satellite GPS radio occultation observation obtained within the storm path (solid) and the temperature profile from MSIS-90 (dashed) for comparison. The profile's large double tropopause implies either the presence of gravity waves or a possible wave generation source.

electric field dominates during first hour of the period shown. The lower altitudes exhibit a strong southward field first. By 0312 UT all but the 293, 553, 590 km altitudes have fields nearly due south. From 0207 to 0312 UT, when TS Odette is 550–560 km northeast of AO, electric field magnitudes reached 4–5 mV/m for altitudes below 370 km. The horizontal electric field slowly shifts to a more northerly direction beginning with the higher-altitude (latitude) measurements.

[19] The zonal and meridional electric fields shown as a function of time in Figure 6 can be compared to typical nighttime fields. Normally, the electric field is directed slightly northward or southward during that period with a magnitude much less than 2 mV/m [*Richmond et al.*, 1980; *Ganguly et al.*, 1987]. Even during intense geomagnetic storms, the meridional electric field does not normally exceed 2.5 mV/m [*Pi et al.*, 2000]. Further, the 7–8 December observations show a direction reversal occurring earlier than commonly observed.

[20] Overall, the observations presented prior to 0400 UT are atypical and cannot be explained by auroral activity or prompt penetration electric fields. Auroral activity can create localized heating and produce TIDs that propagate equatorward, producing *F* region perturbations. However, typical speeds for such TIDS are on the order of 100–200 m/s leading to transient times from the auroral zone to midlatitudes of 5–10 hours. The Kp activity shown in Figure 2 for the 5–10 hours prior to the AO observation show a Kp value of 3+. This value is right at the threshold between quiet and disturbed conditions as determined from the statistical study by *Earle and Kelley* [1987].

[21] Very large variations in magnitude over the observation period are measured in the eastward drift. A possible explanation is the passage of the tropical storm to the north. Coupling between the tropospheric storm and the ionosphere could occur through two mechanisms: electric fields or gravity waves. Both options are examined in detail below for the feasibility of producing the observed ionospheric observations.

[22] Tropical Storm Odette was not strongly cyclonic and did not have a distinct pressure center. Thus the most significant gravity wave generators associated with Odette was the intense convection cells located on the leading side of the storm center. This is the reason convection cells are the focus in the following discussion, and gravity wave generation by vortex motion is only briefly mentioned.

[23] The intense convection cells eastward of the storm center are identified using satellite-based microwave imagery (courtesy of NRL-Monterey; http://www.nrlmry.navy. mil/sat_products.html). Very strong convective upwellings result in much colder cloud top temperatures as compared to the ambient air. Satellite images of cloud tops are used to identify horizontal convective cell size. The convection cells associated with Odette had horizontal sizes between 20 and 35 km. Numerical simulations have reinforced observations that intense convection cells with upwelling plumes are capable of penetrating higher than typical tropopause altitudes causing troposphere/stratosphere mixing [*Lane et al.*, 2001]. Gravity waves generated by the convection cells within the storm [*Röttger*, 1977; *Vadas and Fritts*, 2004, 2006] as well as the motion of the low pressure vortex system [*Saffman*, 1995] could propagate upwards into the lower thermosphere and bottomside *F* region. This leads to plasma motion parallel to the magnetic field that then creates polarization electric fields leading to atypically large perpendicular drifts. Gravity waves generated by convection tend to produce waves that propagate asymmetrically in the direction opposite to the storms' motion [*Beres et al.*, 2002]. The large observed plasma drifts occur following the storm, which agrees with previously observed generation of hurricane, produced gravity waves. *Waldock and Jones* [1997] showed that midlatitude ionospheric disturbances most likely caused by tropospheric gravity waves occur within 1250 km horizontally of the generation source. More recently, a modeling study by *Vadas and Fritts* [2006] showed that severe thunderstorms are capable of affecting neutral perturbation velocities up to a 1500 km distance horizontally from the storm. The occultations with the stratospheric gravity wave activity and *F* region scintillation shown in Table 1 all occurred within 1200 km of the storm center and the convection cells.

[24] A simplified calculation helps quantify the characteristics of possible storm-generated gravity waves. Assume that the gravity wave generation sources are the intense convection cells within 100 km east of the storm eye and assume a propagation direction 20° from the horizontal. Also, assume an isothermal atmosphere. The simplified orientation of the storm to the magnetic field is shown in the right panel of Figure 1. Since the convection cells are located along the storm path, the center of the storm in the right panel of Figure 1 can represent the location of the sources. The convection cells pass 293°E longitude near 1730 UT. According to Figure 1, the magnetic field lines

that intersect the radar volume near points A−B cross over the storm eye at altitudes between 100 and 200 km. The vertical group velocities of the waves that reach those altitudes by the observing time 0100 UT range between 13 and 26 m s^{-1}. The ground-based period of the wave observed by AO at 367 km (Figure 5) is approximately 90 min. If background neutral wind effects are ignored, it can be assumed that the intrinsic frequency equals the ground-based frequency. Using the simplified gravity wave dispersion relation the vertical wavelength can be calculated [*Gossard and Hooke*, 1975]:

$$\lambda_z \approx \frac{\omega_I \lambda_x}{N} \qquad (1)$$

where ω_I is the intrinsic frequency, N is the Brunt-Vaisala frequency, λ_x is wavelength in the x direction. Using a value of 0.01 for the Brunt-Vaisala frequency in the thermosphere and horizontal wavelengths of 20−600 km, the vertical wavelength at 100−200 km altitude ranges between 2 and 70 km, ignoring dissipative filtering effects.

[25] The primary difficulty in relating the observed ionospheric perturbations to gravity wave source regions in the troposphere is the lack of accurate information describing the neutral atmosphere over the altitude range of interest, and the unknown initial gravity wave characteristics. However, modeling and limited observational studies have begun to provide a range of parameter values for gravity waves located first in the troposphere and propagating to the thermosphere [*Hung and Smith*, 1978; *Vadas and Fritts*, 2006]. HF radar observations have measured gravity waves associated with a hurricane with periods of 20−25 min and horizontal phase velocities of 100−200 m s^{-1} at altitudes between 200 and 250 km [*Hung and Smith*, 1978]. Unfortunately, the parameters measured in the *Hung and Smith* [1978] study cannot be directly compared to our calculations because of the unknown initial atmospheric conditions during our experiment.

[26] Numerical simulation studies can provide a more versatile tool to assess the probability of tropospheric forced waves reaching the ionosphere. In the special case described in the study by *Vadas and Fritts* [2006], it was shown that gravity waves with vertical wavelengths of 25−75 km reach altitudes from 125−200 km before dissipating. Thus the vertical wavelength estimates associated with Odette's passage are reasonable.

[27] Gravity waves can produce F region disturbances if they reach either the E region (100 km) or the bottomside of the F region (~200 km). Gravity waves can directly perturb the F region by propagating to at least 200 km or the bottomside of the F region. Once there scintillation, as observed by GPS occultation listed in Table 1, may be produced via the nonlinear Perkins instability [*Huang et al.*, 1994]. Gravity waves reaching the E region may also produce F region disturbances. Once the waves reach 100−200 km, the neutral waves perturb the limited plasma present producing electric field variations that are then mapped to the higher altitude within the radar observing volume. Recent work by *Cosgrove and Tsunoda* [2004] proposes an explanation of F region instabilities that are the result of electrical coupling to Es layers.

[28] In addition to gravity wave effects, intense thunderstorm cells are capable of producing electric fields that reach ionospheric altitudes. There are several phenomena associated with thunderstorms that are known to couple to the lower ionosphere [*Rycroft*, 2006]. These include red sprites, blue jets, and elves. These phenomena are extremely short transient events lasting less than a second that are, in general, rare occurrences. The DE-2 satellite observed a transient electric field, most likely due to lightning discharges, above Hurricane Debbie in 1982 [*Burke et al.*, 1992]. Additionally, sounding rocket data of the ionosphere above an active thunderstorm measured perturbations on the background electric field that lasted 10−20 ms but no overall changes in the DC field [*Kelley et al*, 1985; *Holzworth et al.*, 1985]. Thus any effects on the ionosphere due to lightning phenomena are very short-lived. The large magnitude and varying plasma drifts observed during Odette occurred over several hours and are not likely to be produced through direct electrical coupling between the intense convection cells and the ionosphere.

[29] Hurricanes most likely exhibit electric fields greater than nonstorm periods. Unfortunately, there are no measurements of electric fields within or directly above hurricanes [*Krasilnikov*, 1997]. Recent studies have investigated DC electric fields at ionospheric altitudes over typhoons [*Sorokin et al.*, 2005]. Using the COSMOS-1809 satellite with an orbit near 950 km, Sorokin et al. observed southwest directed electric fields of nearly 25 mV/m at a spatial resolution of 20 km. These values are much larger than observed at F region altitudes by AO. However, the AO observations were made following the passage of the storm and not directly above. Therefore electric field coupling between the storm and the ionosphere cannot be completely discounted.

4. Summary

[30] The local ionosphere above the Arecibo Observatory has been observed following the passage of a nearby tropical storm. Additionally, GPSRO profiles provide information on conditions below 25 km in the storm vicinity. GPSRO data showed an increase in gravity wave activity in the stratosphere near the storm. Large double tropopause conditions indicate gravity wave formation associated with the storm. Arecibo observations made when Odette was located within 600 km of the radar showed surprising variations in the F region plasma drift, with all three components having significant altitude and temporal fluctuations. Large drifts in the zonal direction, atypical for similar conditions, were observed during most of the night. The amplitude spread in the zonal drift is more than twice that observed under similar magnetic conditions a month earlier. The calculated horizontal electric field component varied abnormally when the storm center was closer than 570 km to AO. After the first hour of operation when the storm passed beyond approx. 570 km, the horizontal electric field component returned to more smoothly varying condition. This evidence suggests that Tropical Storm Odette produced measurable effects on the F region ionosphere by producing gravity waves that propagated to a minimum altitude of 100 km. However, continuous and comprehen-

sive radar observations along with gravity wave ray-tracing algorithms are necessary to confirm that such atypical ionospheric observations are the result of tropospheric forcing.

References

Bauer, S. J. (1958), An apparent ionospheric response to the passage of hurricanes, *J. Geophys. Res.*, *63*, 265–269.

Beres, J. H., M. J. Alexander, and J. R. Holton (2002), Effects of tropospheric wind shear on the spectrum of convectively generated gravity waves, *J. Atmos. Sci.*, *59*, 1805–1824.

Boeck, W. L., O. H. Vaughan Jr., R. J. Blakeslee, B. Vonnegut, M. Brook, and J. McKune (1995), Observations of lightning in the stratosphere, *J. Geophys. Res.*, *100*, 1465–1475.

Burke, W. J., T. L. Aggson, N. C. Maynard, W. R. Hoegy, R. A. Hoffman, R. M. Candy, C. Liebrecht, and E. Rodgers (1992), Effects of a lightning discharge detected by the DE 2 satellite over Hurricane Debbie, *J. Geophys. Res.*, *97*, 6359–6367.

Cosgrove, R. B., and R. T. Tsunoda (2004), Instability of the E-F coupled nighttime midlatitude ionosphere, *J. Geophys. Res.*, *109*, A04305, doi:10.1029/2003JA010243.

Earle, G. D., and M. C. Kelley (1987), Spectral studies of the sources of ionospheric electric fields, *J. Geophys. Res.*, *92*, 213–224.

Fejer, B. G. (1993), F region plasma drifts over Arecibo: Solar cycle, seasonal, and magnetic activity effects, *J. Geophys. Res.*, *98*, 13,645–13,652.

Fejer, B. G., and J. T. Emmert (2003), Low-latitude ionospheric disturbance electric field effects during the recovery phase of the 19–21 October 1998 magnetic storm, *J. Geophys. Res.*, *108*(A12), 1454, doi:10.1029/2003JA010190.

Ganguly, S., R. A. Behnke, and B. A. Emery (1987), Average electric field behavior in the ionosphere above Arecibo, *J. Geophys. Res.*, *92*, 1199–1210.

Goodwin, G. L. (1980), An association between atmospheric disturbances at ground level and in the ionosphere, *J. Atmos. Terr. Phys.*, *42*, 899–906.

Gossard, E. E., and W. H. Hooke (1975), *Waves in the Atmosphere*, 112 pp., Elsevier, New York.

Hagfors, T., and R. A. Behnke (1974), Measurements of three-dimensional plasma velocities at the Arecibo Observatory, *Radio Sci.*, *9*, 90–93.

Holton, J. R. (1992), *Introduction to Dynamic Meteorology*, Elsevier, New York.

Holzworth, R. H., M. C. Kelley, C. L. Siefring, L. C. Hale, and J. D. Mitchell (1985), Electrical measurements in the atmosphere and the ionosphere over an active thunderstorm: 2. Direct current electric fields and conductivity, *J. Geophys. Res.*, *90*, 9824–9830.

Huang, C-S., C. A. Miller, and M. C. Kelley (1994), Basic properties and gravity wave initiation of the mid-latitude F region instability, *Radio Sci.*, *29*, 395.

Hung, R. J., and J. P. Kuo (1978), Ionospheric observation of gravity waves associated with Hurricane Eloise, *J. Geophys.*, *45*, 67–80.

Hung, R. J., and R. E. Smith (1978), Ray tracing of gravity waves as a possible warning system for tornadic storms and hurricanes, *J. Appl. Meteorol.*, *17*, 3–11.

Kazimirovsky, E., M. Herraiz, and B. A. de la Morena (2003), Effects on the ionosphere due to phenomena occurring below it, *Surv. Geophys.*, *24*, 139–184.

Kelley, M. C. (1997), In situ ionospheric observations of severe weather–related gravity waves and associated small-scale plasma structure, *J. Geophys. Res.*, *102*, 329–335.

Kelley, M. C., C. L. Siefring, R. F. Pfaff, P. M. Kitner, M. Larsen, R. Green, R. H. Holzworth, L. C. Hale, J. D. Mitchell, and D. Le Vine (1985), Electrical measurements in the atmosphere and the ionosphere over an active thunderstorm: 1. Campaign overview and initial ionospheric results, *J. Geophys. Res.*, *90*, 9815–9823.

Krasilnikov, E. Y. (1997), Electromagnetohydrodynamic nature of tropical cyclones, hurricanes, and tornadoes, *J. Geophys. Res.*, *102*, 13,571–13,580.

Lane, T. P., M. J. Reeder, and T. L. Clark (2001), Numerical modeling of gravity waves generated by deep tropical convection, *J. Atmos. Sci.*, *58*, 1249–1274.

Larsen, M. F., W. E. Swartz, and R. F. Woodman (1982), Gravity-wave generation by thunderstorms observed with a vertically-pointing 430 MHz radar, *Geophys. Res. Lett.*, *9*, 571–574.

Lastovicka, J. (2006), Forcing of the ionosphere by waves from below, *J. Atmos. Sol. Terr. Phys.*, *68*, 479–497, doi:10.1016/j.jastp.2005.01.018.

Mathews, J. D. (1998), Sporadic E: current views and recent progress, *J. Atmos. Sol. Terr. Phys.*, *60*, 413–435.

Mazano, J. R., S. M. Radicella, M. M. Zossi de Artigas, A. N. Filippi de Manzano, and A. H. Cosio de Ragone (1998), Troposphere-ionosphere interaction during tropospheric mesoscale convective complexes events, *J. Atmos. Sol. Terr. Phys.*, *60*, 585–594.

Pi, X., M. Mendillo, W. J. Hughes, M. J. Buonsanto, D. P. Sipler, J. Kelly, Q. Zhou, G. Lu, and T. J. Hughes (2000), Dynamical effects of geomagnetic storms and substorms in the middle-latitude ionosphere: An observational campaign, *J. Geophys. Res.*, *105*, 7403–7417.

Richmond, A. D., et al. (1980), An empirical model of quiet-day ionospheric electric fields at middle and low latitudes, *J. Geophys. Res.*, *85*, 4658.

Röttger, J. (1977), Atmospheric gravity waves generated by penetrative cumulus convection in the tropics, paper presented at 11th Technical Conference on Hurricanes and Tropical Meteorology, Am. Meteorol. Soc., Miami Beach, Fla.

Rycroft, M. J. (2006), Electrical processes coupling the atmosphere and ionosphere: An overview, *J. Atmos. Sol. Terr. Phys.*, *68*, 445–456, doi:10.1016/j.jastp.2005.04.009.

Saffman, P. G. (1995), *Vortex Dynamics*, Cambridge Univ. Press., New York.

Sorokin, V. M., N. V. Isaev, A. K. Yaschenko, V. M. Chmyrev, and M. Hayakawa (2005), Strong DC electric field formation in the low latitude ionosphere over typhoons, *J. Atmos. Sol. Terr. Phys.*, *67*, 1269–1279, doi:10.1016/j.jastp.2005.06.014.

Sulzer, M. P., N. Aponte, and S. A. Gonzalez (2005), Application of linear regularization methods to Arecibo vector velocities, *J. Geophys. Res.*, *110*, A10305, doi:10.1029/2005JA011042.

Uccellini, L. W., D. Keyser, K. F. Brill, and C. H. Wash (1985), The Presidents' Day cyclone of 18–19 February 1979: influence of upstream trough amplification and associated tropopause folding on rapid cyclogenesis, *Mon. Weather Rev.*, *113*, 962–988.

Vadas, S. L., and D. C. Fritts (2004), Thermospheric responses to gravity waves arising from mesoscale convective complexes, *J. Atmos. Solar Terr. Phys.*, *66*, 781–804, doi:10.1016/j.jastp.2004.01.025.

Vadas, S. L., and D. C. Fritts (2006), The influence of solar variability on gravity wave structure and dissipation in the thermosphere from tropospheric convection, *J. Geophys. Res.*, *111*, A10S12, doi:10.1029/2005JA011510.

Waldock, J. A., and T. B. Jones (1997), Source regions of medium scale travelling ionospheric disturbances observed at mid-latitudes, *J. Atmos. Terr. Phys.*, *49*, 105–114.

Wickert, J., et al. (2001), Atmosphere sounding by GPS radio occultation: first results from CHAMP, *Geophys. Res. Lett.*, *28*, 3263–3266.

Yokoyama, N., and Y. Kamide (1997), Statistical nature of geomagnetic storms, *J. Geophys. Res.*, *102*, 14,215–14,222.

―――――――――――

N. Aponte and M. Sulzer, Space and Atmospheric Sciences, Arecibo Observatory, HC-03 Box 53995, Arecibo, PR 00612, USA.

R. L. Bishop and G. S. Peng, The Aerospace Corporation, P. O. Box 92957, El Segundo, CA 90009-2957, USA. (rebecca.l.bishop@aero.org)

G. D. Earle, William B. Hanson Center for Space Sciences, University of Texas at Dallas, WT-15, Richardson, TX 75083-0688, USA.

M. F. Larsen, Department of Physics, Clemson University, Kinard Laboratory, Clemson, SC 29634, USA.